

Large negative magnetoresistance of a nearly Dirac material: Layered antimonide EuMnSb₂Changjiang Yi,^{1,2} Shuai Yang,^{1,2} Meng Yang,^{1,2} Le Wang,^{1,2} Yoshitaka Matsushita,³ Shanshan Miao,¹ Yuanyuan Jiao,^{1,2} Jinguang Cheng,^{1,2} Yongqing Li,^{1,2} Kazunari Yamaura,^{4,5,*} Youguo Shi,^{1,2,†} and Jianlin Luo^{1,2,6}¹Beijing National Laboratory for Condensed Matter Physics and Institute of Physics, Chinese Academy of Sciences, Beijing 100190, China²School of Physical Sciences, University of Chinese Academy of Sciences, Beijing 100190, China³Materials Analysis Station, National Institute for Materials Science, 1-2-1 Sengen, Tsukuba, Ibaraki 305-0047, Japan⁴Research Center for Functional Materials, National Institute for Materials Science, 1-1 Namiki, Tsukuba, Ibaraki 305-0044, Japan⁵Graduate School of Chemical Sciences and Engineering, Hokkaido University, North 10 West 8, Kita-ku, Sapporo, Hokkaido 060-0810, Japan⁶Collaborative Innovation Center of Quantum Matter, Beijing 100190, China

(Received 6 June 2017; revised manuscript received 3 October 2017; published 1 November 2017)

Single crystals of EuMnSb₂ were successfully grown and their structural and electronic properties were investigated systematically. The material crystallizes in an orthorhombic-layered structure (space group: *Pnma*, No. 62) comprising a periodic sequence of -MnSb/Eu/Sb/Eu/- layers (~1 nm in thickness), and massless fermions are expected to emerge in the Sb layer, by analogy of the candidate Dirac materials EuMnBi₂ and AMn*Pn*₂ (*A* = Ca or Sr or Ba, *Pn* = Sb or Bi). The magnetic and specific heat measurements of EuMnSb₂ suggest an antiferromagnetic ordering of Eu moments near 20 K. A characteristic hump appears in the temperature-dependent electrical resistivity curve at ~25 K. A spin-flop transition of Eu moments with an onset magnetic field of ~15 kOe (at 2 K) was observed. Interestingly, EuMnSb₂ shows a negative magnetoresistance (up to -95%) in contrast to the positive magnetoresistances observed for EuMnBi₂ and AMn*Pn*₂ (*A* = Ca or Sr or Ba, *Pn* = Sb or Bi), providing a unique opportunity to study the correlation between electronic and magnetic properties in this class of materials.

DOI: [10.1103/PhysRevB.96.205103](https://doi.org/10.1103/PhysRevB.96.205103)**I. INTRODUCTION**

Topological materials attract significant attention because they demonstrate exotic properties such as nonzero Berry phase, quantum Hall effect, and large magnetoresistance (MR) [1–3]. The exotic features have been characterized as Dirac (Weyl) fermions, which possess small effective mass and are highly mobile. The massless fermion materials are therefore expected to be useful in engineering advanced devices for high-speed electronic circuits and quantum computing.

In past years, theoretical studies predicted linear energy dispersion near the Fermi surface of a class of materials. Indeed, these materials' properties were well characterized experimentally by linear energy dispersion as Dirac or Weyl fermions, as reported for HgTe [4,5], Na₃Bi [6], Cd₃As₂ [6–9], and TaAs [10,11]. As the linear energy dispersion is strongly coupled with the transport properties, a transport study has been recognized as an effective method to search for additional topological materials, in addition to angle-resolved photoemission spectroscopy.

Recent theoretical studies indicate that the layered manganese pnictides AMn*Pn*₂ (*A* = Ca or Sr or Ba, *Pn* = Sb or Bi) host an anisotropic Dirac cone near the Fermi surface [12,13]. The bulk properties are expected to possess a large positive MR and manifest quantum oscillations in an increasing magnetic field (*H*). Experimental studies of CaMnBi₂ [14–19], SrMnBi₂ [16,17,20,21], BaMnBi₂ [22], and BaMnSb₂ [23,24] supported these possibilities. In addition, similar properties have been experimentally observed for related compounds like EuMnBi₂ [25,26], YbMnBi₂ [27], LaAgSb₂

[28,29], and LaAgBi₂ [30], making them promising candidates for Dirac materials. The aforementioned compounds share either a Bi or Sb square layer, in which low-mass Dirac (Weyl) fermions emerge [12]. As the common crystal structure comprises a periodic sequence of -Mn*Pn*/*A*/*Pn*/*A*/- layers (~1 nm in thickness) along a crystallographic direction, these compounds can be regarded as bulk matter of massless fermions, which offers a significant merit to develop technological applications.

More specifically, the local structure environment of a Bi or Sb layer (slightly distorted to a zigzag chain in the orthorhombic lattice, *b/c* ~ 0.991 [31]) has a significant impact on the anisotropic Dirac cone according to the theoretical studies, suggesting that massless fermions are unlikely to emerge in orthorhombic SrMnSb₂. However, recent experimental studies clearly demonstrated remarkable Dirac features of SrMnSb₂ [32,33]. Therefore, the nature of the Dirac features of AMn*Pn*₂ with a zigzag chain net remains highly controversial.

In this study, we succeeded in growing a single crystal of EuMnSb₂ (*b/c* ~ 0.994) (see Table I). Unlike isostructural SrMnSb₂, semiconductinglike behavior was found in EuMnSb₂, with an estimated activation energy of 30.1(4) meV. Interestingly, a negative MR (up to -95%) was observed at low temperatures. We report details of the transport properties of EuMnSb₂ that are qualitatively different from the properties of other AMn*Pn*₂ materials. In particular, negative MR has not been reported for this series as far as we knew. Experimental observation of EuMnSb₂, therefore, promotes drawing a comprehensive picture of the peculiar transport properties of AMn*Pn*₂, which is possibly a bulk Dirac material.

II. EXPERIMENTAL DETAILS

Single crystals of EuMnSb₂ were grown out of a Sn flux. Starting materials Eu (ingot, 99.9%, Purui Advanced Material

*ygshi@iphy.ac.cn

†YAMAURA.Kazunari@nims.go.jp

TABLE I. Crystal structure and magnetoresistance of $AMnPn_2$ and related compounds.

Compounds	Space group	Magnetoresistance (%)	Effective mass (m_e) ^a	Reference
EuMnSb ₂	<i>Pnma</i>	−95 (2 K, 90 kOe)		This work
EuMnBi ₂	<i>I4/mmm</i>	600 (5 K, 120 kOe)		[25,26]
YbMnBi ₂	<i>P4/nmm</i>	234 (2 K, 90 kOe)		[27]
LaAgBi ₂	<i>P4/nmm</i>	1200 (2 K, 90 kOe)	0.056	[30]
LaAgSb ₂	<i>P4/nmm</i>	550 (2 K, 80 kOe)	0.16	[28,29]
BaMnBi ₂	<i>I4/mmm</i>	300 (2 K, 120 kOe)	0.105	[22]
BaMnSb ₂	<i>I4/mmm</i>		0.052–0.058	[23]
SrMnBi ₂	<i>I4/mmm</i>	110 (2 K, 90 kOe)	0.29	[20]
SrMnSb ₂	<i>Pnma</i>	135 (30 K, 160 kOe)	0.069	[33]
CaMnBi ₂	<i>P4/nmm</i>	44 (2 K, 90 kOe)	0.35	[17–19]

^a m_e : mass of free electron.

Technology Co. Ltd., Beijing, China), Mn (pieces, 99.98%, Alfa Aesar), Sb (pills, 99.999%, Alfa Aesar), and Sn (pills, 99.999%, Alfa Aesar) were mixed in an Ar-filled glove box at a molar ratio of Eu : Mn : Sb : Sn = 1 : 1 : 2 : 10. The mixture was placed in an alumina crucible, which was then sealed in an evacuated quartz tube. The tube was heated up to 1000 °C over 10 h and then dwelt for 20 h. Then, the tube was slowly cooled down to 600 °C at a rate of 2.5 °C/h followed by separating the crystals from the Sn flux by centrifuging. Shiny crystals with a typical dimension of 2 × 2 × 1 mm were obtained on the bottom of the crucible. The millimeter-sized crystals are square-plate-like with distinct right angles. The crystal was rather stable in air.

To investigate the crystalline structure, single-crystal x-ray diffraction (XRD) study was carried out using a Rigaku Saturn charge-coupled device diffractometer equipped with VariMax confocal optics for MoK_α radiation ($\lambda = 0.71073 \text{ \AA}$). The single-crystal XRD data were refined by a full-matrix least-squares method on F^2 using the SHELXL-2014/7 program [34]. The chemical composition of selected crystals was analyzed by energy-dispersive x-ray spectroscopy (EDX) in a Hitachi S-4800 at an accelerating voltage of 15 kV and electro-probe microanalyzer (EPMA) in a JEOL JXA-8900 at an accelerating voltage of 15 kV.

A selected crystal was used for magnetic and specific heat capacity (C_p) measurements. The magnetic properties were measured in a Magnetic Properties Measurement System (MPMS-III, Quantum Design Inc.) with a superconducting quantum interference device–vacuum-tube voltmeter option. Magnetic susceptibility (χ) was measured at temperatures between 2 and 300 K in fixed applied magnetic fields of 10 and 50 kOe under field-cooling and zero-field-cooling conditions. Isothermal magnetization (M - H) at crystallographic directions perpendicular and parallel to the a axis was measured in a sweeping field from −50 to 50 kOe. The C_p was measured by a thermal-relaxation method from 2 to 300 K in a fixed magnetic field in a Physical Property Measurement System (PPMS, Quantum Design Inc.). Apiezon N grease was used to thermally connect the crystal to a holder stage. The applied field was parallel to the a axis during the heat capacity measurement. ac magnetic susceptibility was measured in the PPMS with and without in-fixed applied magnetic fields (parallel to the a axis; 300 Oe and 10 kOe). The amplitude and frequency of ac magnetic field were in a range of 10 and 15 Oe, 133 and 9999 Hz, respectively.

Longitudinal resistivity (ρ_{xx}) and MR were measured in the PPMS in a configuration that four platinum wires were fixed on a crystal by silver epoxy. The MR was defined by $\text{MR}(\%) = \frac{R(H) - R(H=0)}{R(H=0)} \times 100\%$. Hall resistivity (ρ_{xy}) was measured in a JANIS He-4 system by a six-terminal configuration method in a sweeping field from −90 to 90 kOe at various fixed temperatures.

III. RESULTS AND DISCUSSION

A. Crystal structure

The single-crystal XRD study revealed that the compound EuMnSb₂ crystallizes in an orthorhombic structure with lattice parameters $a = 22.5726(12) \text{ \AA}$, $b = 4.3850(3) \text{ \AA}$, and $c = 4.4095(2) \text{ \AA}$. The space group is *Pnma* (No. 62), identical to that of SrMnSb₂ [31]. The refined parameters are summarized in Table II as well as Tables S1 and S2 in Supplemental Material [35]. The ratio of the lattice parameters b/c is 0.994, which is comparable to that of SrMnSb₂ ($b/c = 0.991\text{--}0.989$ [31,32]). Note that the orthorhombic distortion has been observed only for SrMnSb₂ and EuMnSb₂ in the family of $AMnPn_2$ (see Table I for example).

Based on the refinement, Fig. 1(a) shows a schematic drawing of the crystal structure featured by a stacking of $-MnPn/Al/Pn/Al/-$ layers along the a axis. This is a common feature of $AMnPn_2$, regardless of whether the symmetry is tetragonal or orthorhombic. The Sb layer (sandwiched by the

TABLE II. Atomic coordinates and equivalent isotropic thermal parameters of EuMnSb₂.^a

Atoms	WP ^b	g	x	y	z	U_{eq}
Eu	4c	1	0.38637(2)	0.2500	0.76977(5)	0.01049(6)
Mn	4c	1	0.24970(3)	1.2500	0.27005(14)	0.01092(10)
Sb1	4c	1	0.32532(2)	0.7500	0.27005(6)	0.00968(6)
Sb2	4c	1	0.49905(2)	0.2500	0.27819(6)	0.01059(6)

^aSpace group: *Pnma* (orthorhombic, No. 62); lattice constants $a = 22.5851(11) \text{ \AA}$, $b = 4.3768(2) \text{ \AA}$, $c = 4.4122(2) \text{ \AA}$; cell volume = $436.154(2) \text{ \AA}^3$; $d_{cal} = 6.8615(5) \text{ g cm}^{-3}$; $Z = 4$; and the final $R1$ value is 5.55%. Additional details of crystallographic and refinement information and anisotropic displacement parameters (Å^2) are summarized in Supplemental Material, Tables S1 and S2 [35].

^bWyckoff position.

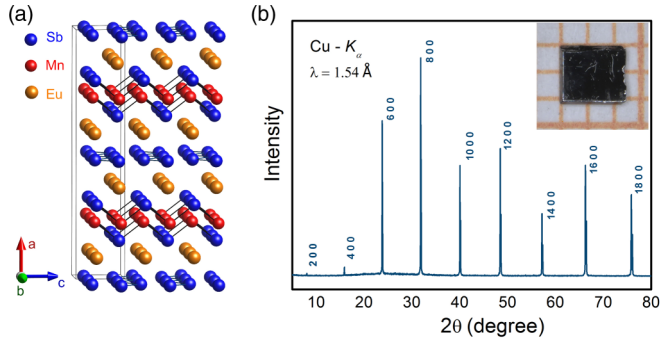


FIG. 1. (a) Crystal structure of EuMnSb_2 , revealing a stacking sequence of $-\text{MnSb}/\text{Eu}/\text{Sb}/\text{Eu}/-$ (~ 1 nm in thickness). The Sb atoms form a zigzag chain net in a layer. (b) XRD pattern of a flat crystal shows only the $h00$ peaks, indicating that the flat face is a bc plane. The inset is a photograph of a typical crystal (the back square is 1×1 mm 2).

Eu layers) comprises Sb zigzag chains running along the b axis, as found in SrMnSb_2 .

Figure 1(b) shows a typical XRD profile ($\text{Cu } K_\alpha$) of a flat crystal. It shows only $h00$ peaks, indicating that the flat plane is a bc plane. Besides, any trace of impurity was undetected. The inset is a photograph of the crystal. The back square of 1×1 mm indicates the size of the crystal. The composition of a selected crystal (Supplemental Material, Fig. S1 [35]) was found to be $\text{Eu} : \text{Mn} : \text{Sb} : \text{Sn} = 24.8 : 25.2 : 49.2 : 0.73$ from EPMA, confirming the stoichiometry of the crystal. The possible Sn contamination is lower than 0.03 moles per formula unit (EuMnSb_2). Details, including the EDX results, are presented in Supplemental Material, Table S3 [35].

B. Magnetic properties

Magnetic properties of a flat-plate-like crystal of EuMnSb_2 were measured: Fig. 2(a) shows the temperature and direction dependence of χ . Although an obvious indication of an antiferromagnetic (AFM) ordering of Mn magnetic moments was not seen up to 400 K (see Supplemental Material, Fig. S2 [35] as well), it is reasonable to assume that an AFM order of the moments is established above 300 K. This is because (i) the C_p - T curve (shown below) has no anomalies below 300 K (except anomalies below 25 K), (ii) a magnetic transition associated with the Mn magnetic moments was clearly detected by a C_p - T measurement in other AMnPn_2 compounds, although the accompanying anomalies in χ - T curves were not noticeable [26,27], and (iii) the series of AMnPn_2 shows AFM transition at nearly constant temperatures, regardless of the selection of A and Pn ; for example, 310 K (EuMnBi_2 [25,26]), 290 K (YbMnBi_2 [27]), 280 K (SrMnBi_2 [20]), and 270 K (CaMnBi_2 [18]). Note that Yb magnetic moments do not have a major impact on the ordering of Mn magnetic moments in YbMnBi_2 [27], supporting the assumption.

Although no ordering of Mn magnetic moments (>300 K) was detected for EuMnSb_2 throughout our experimental measurements, another magnetic ordering was clearly detected at ~ 20 K. Below the ordering temperature, the dependencies of crystal direction as well as magnitude of magnetic field

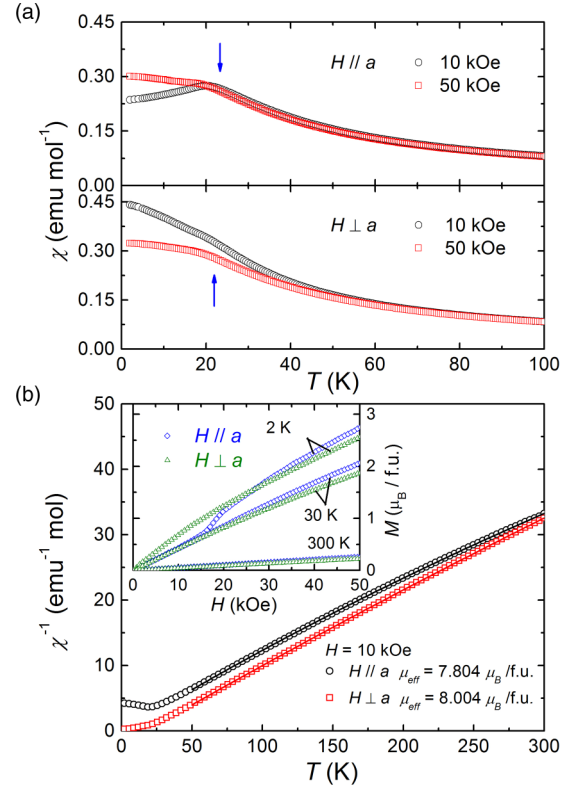


FIG. 2. (a) Temperature and magnetic field dependencies of χ of a single crystal of EuMnSb_2 , measured in parallel and perpendicular directions of a axis to the field. (b) Temperature dependence of χ^{-1} in a field of 10 kOe. Solid curves are simulated by the Curie-Weiss law. The inset shows isothermal magnetizations measured in parallel and perpendicular directions of a axis to the field at various temperatures.

were obvious on the χ - T curves. The dependencies indicate that an A -type AFM order is likely to be established below ~ 20 K; in other words, a ferromagnetic (FM) layer is antiferromagnetically coupled with the neighboring FM layers. This anomaly likely reflects an establishment of the AFM order of the divalent Eu ($4f^7$; $S = 7/2$, $L = 0$, $J = 7/2$). Curie-Weiss analysis (shown below) supports divalency of Eu. Besides, trivalency of Eu is very unlikely because it is formally nonmagnetic ($4f^6$; $S = 3$, $L = 3$, $J = 0$). The A -type AFM order of Eu magnetic moments is therefore certainly plausible. Note that the ordering of Eu magnetic moment of the related pnictide EuMnBi_2 has been studied by others, and the A -type AFM order of Eu^{2+} magnetic moments was highly anticipated [25,26].

The χ^{-1} vs T plots were fit to the Curie-Weiss law, as shown in Fig. 2(b). The analytical formula, $\chi = \chi_0 + C/(T - T_\theta)$, was used over the temperature range from 50 to 300 K, in which χ_0 , C , and T_θ are the temperature-independent term, Curie constant, and Weiss temperature, respectively. The effective moment defined by $\mu_{\text{eff}} = \sqrt{8C} \mu_B$ was estimated to be $7.80 \mu_B$ ($H // a$) and $8.00 \mu_B$ ($H \perp a$), in good accordance with the theoretical value of $7.94 \mu_B$ for Eu^{2+} ($4f^7$). Although the contribution from the magnetically ordered Mn sublattice to the Curie-Weiss analysis was unclear, Eu magnetic moments should play the major role in the magnetic ordering at ~ 20 K.

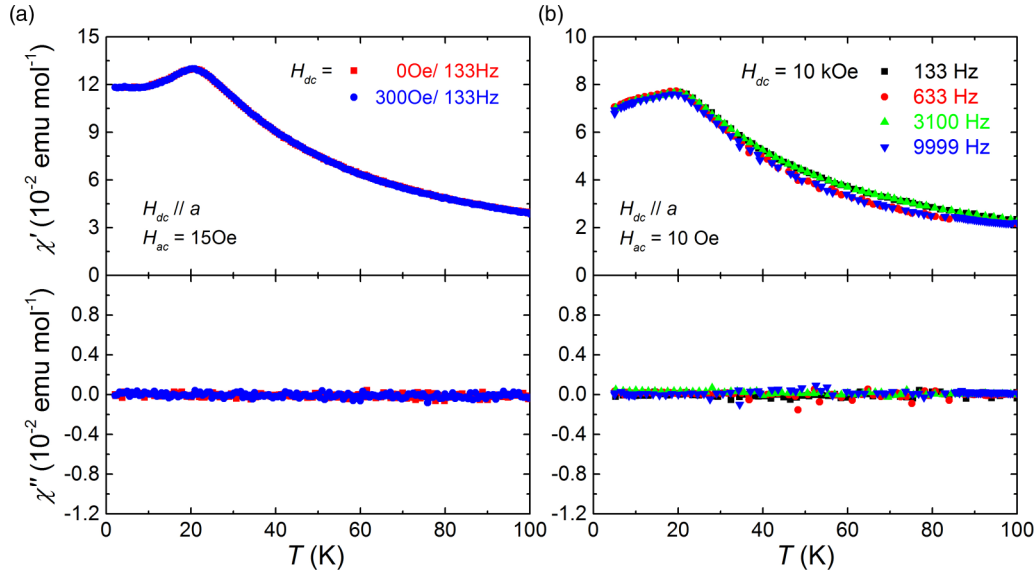


FIG. 3. (a) Real and imaginary components of ac magnetic susceptibility of a single crystal of EuMnSb_2 measured in a fixed magnetic field (H_{dc}) of 0 and 300 Oe, and (b) 10 kOe. The dc magnetic field was applied parallel to the a axis.

The top panel of Fig. 2(a) shows the maximum χ at 20 K (10 kOe, $H//a$), which decreases by $\sim 2.5\%$ on further cooling. The extent of the decrease is remarkably smaller than that in EuMnBi_2 ($\sim 100\%$ [25,26]). The quantitative difference is attributed to a weaker magnetic anisotropy of the AFM state. The direction dependence indicates that the out-of-plane Eu magnetic moments are more weakly coupled than the in-plane moments. The suppressed decrease of χ in a very intense magnetic field (50 kOe, $H//a$) is also qualitatively like that observed for EuMnBi_2 . The bottom panel of Fig. 2(a) shows a small deviation between the curves (10 and 50 kOe, $H\perp a$) that persists even above the transition temperature of 20 K. A comparable feature was not obvious in EuMnBi_2 . Overall, the degree of magnetic anisotropy of EuMnSb_2 seems to be weaker than that of EuMnBi_2 .

To further investigate the magnetic anomaly at ~ 20 K, ac magnetic susceptibility was measured as shown in Figs. 3(a) and 3(b). Unlike CaMn_2Sb_2 [36], any feature connected to possible formation of magnetic polarons is absent. Further experimental confirmation by neutron-diffraction method is necessary to clarify the magnetic nature.

The inset of Fig. 2(b) shows field-induced isothermal magnetization above and below the magnetic transition temperature of ~ 20 K. At 2 K, a spin-flop transition was observed at the onset of 15 kOe, implying deflection of the ordered Eu moments. A similar magnetization anomaly was observed for EuMnBi_2 [25,26] but not for YbMnBi_2 [27,37], implying a common feature of the Eu-based $\text{AMn}Pn_2$. The magnetization of EuMnSb_2 develops with no sign of saturation up to 50 kOe (at 2 K). The feature is outstanding because the Eu^{2+} compounds such as EuCr_2As_2 [38], EuMn_2As_2 [39], and EuMn_2Sb_2 [40] usually saturate near $7\mu_B/\text{Eu}$ (fully ordered Eu^{2+} magnetic moments) below 50 kOe. Besides, nearly equal magnetization curves were observed at $T = 30$ K in the $H//a$ and $H\perp a$ measurements, suggesting a less anisotropic order of Eu magnetic moments. The less anisotropic state may be responsible in part for the large negative MR of EuMnSb_2 shown below. In this study, magnetic interactions between

Eu and Mn moments were not sufficiently revealed, although they may be primarily responsible for the absence of saturated magnetic state below 50 kOe.

C. Specific heat capacity

The C_p vs T curve of EuMnSb_2 was measured, as shown in Fig. 4, over a temperature range of 2 to 300 K. No peaklike anomaly associated with the Mn magnetic moment ordering (like those found for EuMnBi_2 [26] and YbMnBi_2 [27]) was observed. The absence suggests that the ordering of Mn magnetic moments takes place beyond the temperature range (> 300 K). Apart from the ordering of the Mn moments, a distinct anomaly near 20 K was observed; the anomaly is likely associated with the ordering of Eu magnetic moments. The inset (to Fig. 4) is the C_p/T vs T^2 curves measured with various infixed magnetic fields up to 90 kOe. The peak shifts to lower temperatures with increasing applied field, supporting

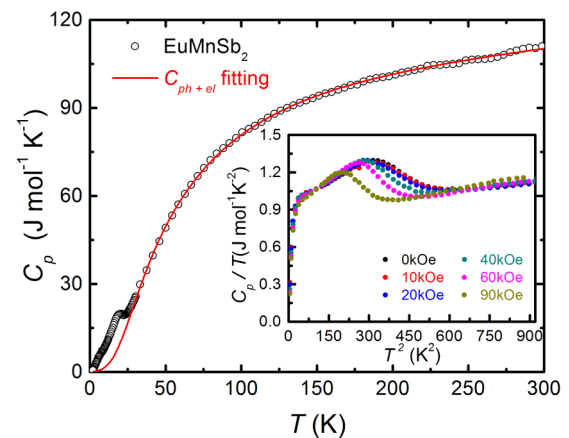


FIG. 4. C_p vs T curve of EuMnSb_2 measured without applying a magnetic field. The fit to the lattice and electrons contributions by the Debye and Einstein models is shown as a solid curve. Inset: an anomaly around 20 K shows a magnetic field dependence.

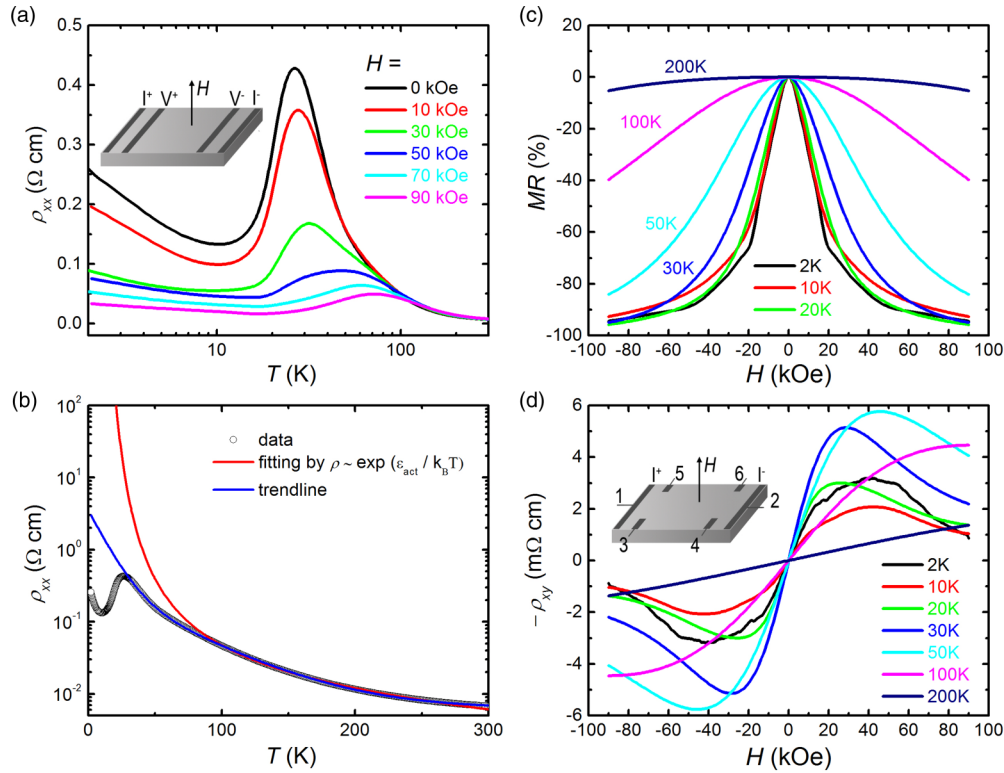


FIG. 5. (a) Plot of temperature dependence of ρ_{xx} of EuMnSb₂ in various magnetic fields parallel to a axis. Inset schematically shows the ρ_{xx} measurement along with four electrical terminals. (b) Estimation of an activation energy by adapting the Arrhenius formula to the zero-field data. (c) MR of ρ_{xx} at various temperatures. (d) Magnetic field dependence of ρ_{xy} at fixed temperatures of 200 K and below. Inset is an image schematically showing the ρ_{xy} measurement with six electrical terminals.

the consideration about the AFM order. The C_p feature is qualitatively similar to that observed for EuMnBi₂ [26], except for the much broader peak.

The Debye-Einstein model [41] was applied to the C_p vs T curve for further analysis, as shown in Fig. 4; the analytical formula is

$$C_{el+ph}(T) = \gamma T + \alpha 9nR \left(\frac{T}{\theta_D} \right)^3 \int_0^{\theta_D/T} \frac{x^4 e^x}{(e^x - 1)^2} dx \\ + (1 - \alpha) 3nR \frac{(\theta_E/T)^2 e^{\theta_E/T}}{(e^{\theta_E/T} - 1)^2},$$

in which θ_D and θ_E are the Debye and Einstein temperatures, respectively, and α is the contribution ratio of the two components. The high-temperature data from 30 to 300 K were utilized in the formula and a curve including the low-temperature part (from 2 to 300 K) was simulated using a set of the refined parameters. The simulation enabled us to roughly separate the lattice contribution from the total C_p . The remaining contribution most likely comes from the magnetic transition; and the transition entropy (ΔS) was roughly estimated to be $13.9 \text{ J mol}^{-1} \text{ K}^{-1}$, slightly lower than the theoretical value of $17.3 \text{ J mol}^{-1} \text{ K}^{-1}$ for the fully ordered Eu²⁺ magnetic moments [$\Delta S = R \ln(2J + 1)$ with $J = 7/2$]. The broad nature of the transition possibly hindered the entropy estimation to some extent.

D. Electronic transport properties

EuMnSb₂ shows semiconductorlike transport properties at high temperatures: ρ_{xx} increases on cooling to ~ 25 K [Fig. 5(a)]. The semiconductorlike behavior contrasts dramatically with the ρ - T behaviors of other AMn Pn_2 compounds (all show metalliclike temperature dependence). The longitudinal resistivity at zero field is fitted to the Arrhenius model $\rho_{xx} \sim \exp(E_a/k_B T)$, where k_B and E_a are the Boltzmann constant and thermal activation energy, respectively, from 150 to 300 K as shown in Fig. 5(b) (see Supplemental Material, Fig. S3 [35] as well). A small E_a of 30.1(4) meV is estimated, indicating a very narrow gap of EuMnSb₂. In addition, the fitting quality at low temperatures (< 80 K) is poor, suggesting that other contributions need to be considered to account for the total electrical conduction.

The ρ_{xx} decreases and then increases again on further cooling. The dramatic character change indeed occurs near the magnetic transition temperature of ~ 20 K; a tight coupling between the magnetic order and charge transport is suggested. A linear increase at low temperatures is indicative of a Kondo-like anomaly, which is usually caused by scattering of magnetic impurities. The peak of the ρ - T curve shifts toward higher temperature with decreased magnitude, consistent with an expected behavior of highly ordered magnetic moments in a higher magnetic field. A similar broad peak was observed for EuSe [42] and CaMn₂Sb₂ [36]; the feature was argued to originate from a formation of magnetic polarons. Unfortunately, no signal of the magnetic polarons is found in EuMnSb₂ [Figs. 3(a) and 3(b)]. The correlation between the

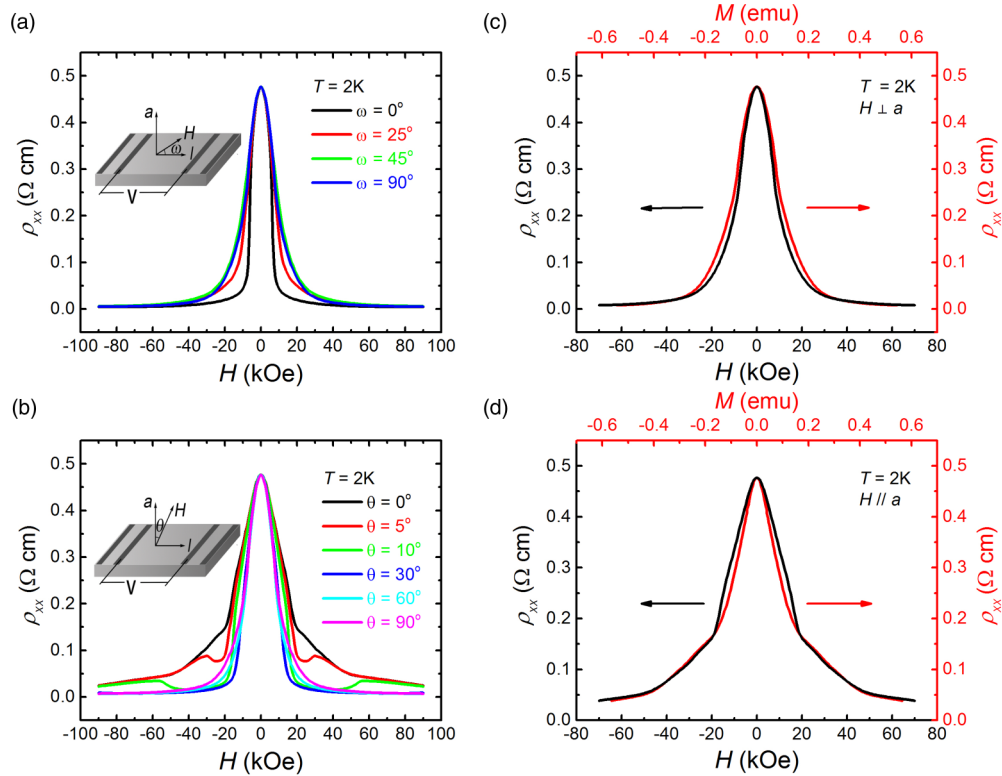


FIG. 6. (a) Applied field dependence of ρ_{xx} of EuMnSb₂ at 2 K with in-plane angles, ω and (b) out-of-plane angles, θ between I and H . The inset in each illustrates the measurement configuration. (c) Comparison of the magnetization dependencies of ρ_{xx} at 2 K for H perpendicular and (d) parallel to a axis.

magnetic order and charge transport of EuMnSb₂ needs further investigation.

The MR was found to be quite negative, as shown in Fig. 5(c); this feature stands out from other observations so far for the AMnPn₂ compounds (see Table I). Among the series, only EuMnSb₂ exhibits a negative MR that is approximately -95% at 90 kOe at low temperatures. Although Sb and Bi are in the same main group, EuMnSb₂ shows a drastically different transport feature from that of EuMnBi₂; for example, EuMnBi₂ exhibits a positive MR ($+600\%$ at 120 kOe) with oscillations owing to the two-dimensional electronic nature [25,26]. The MR features of EuMnSb₂ seem not to directly meet the general expectation for the linear band dispersions near the Fermi surface [30]. An earlier theoretical study suggests that the different properties of EuMnSb₂ are probably caused by the Sb zigzag chain net [12,13]. In other words, the orthorhombic distortion of the lattice has a significant impact on the transport properties. As was already mentioned in the theoretical study, when the lattice goes back to the tetragonal structure on application of physical compression or chemical substitution, the negative MR of EuMnSb₂ may dramatically change to positive MR [12,13].

At low temperatures, an anomalous Hall effect was found in EuMnSb₂ [Fig. 5(d)]. In general, the Hall resistivity of a magnetic compound can be characterized by a linear addition of two components, one for an ordinary Hall effect (OHE) and the other for an anomalous Hall effect (AHE), $\rho_{xy} = R_H B + \mu_0 R_S M$, in which μ_0 is the magnetic permeability constant, M is the magnetization of the subject, and R_H and R_S are the normal and anomalous Hall coefficients, respectively.

The R_S is usually related to ρ_{xx} : (i) R_S is proportional to ρ_{xx} in a high-conductivity regime ($\sigma_{xx} > 10^6 \Omega^{-1} \text{cm}^{-1}$), (ii) R_S is proportional to ρ_{xx}^2 in a metallic regime ($\sigma_{xx} \sim 10^4 - 10^6 \Omega^{-1} \text{cm}^{-1}$), and (iii) R_S is proportional to $\rho_{xx}^{1.6-1.8}$ in a bad-metallic regime ($\sigma_{xx} < 10^4 \Omega^{-1} \text{cm}^{-1}$) [3,43].

In the present study, it was hard to reasonably separate the OHE and AHE components from the total ρ_{xy} ; when EuMnSb₂ is in the activation regime (e.g., at 200 K), the ρ_{xy} is likely to be dominated by the OHE component, indicating a hole-type carrier with a carrier density of $\sim 3.8 \times 10^{18} \text{cm}^{-3}$. However, the sign of the Hall coefficient switches to the opposite with a sweeping magnetic field at low temperatures. The sign change is possibly caused by a modified Fermi surface with developing magnetic order. Note that the ρ_{xy} - H measurements at the R_{3-5} and R_{4-6} terminals [see Fig. S4(a)] are qualitatively and quantitatively similar, and furthermore, two independent crystals show similar ρ_{xy} - H behaviors as well [see Fig. S4(b)]. Therefore, the uniformity of the crystals is high. The anomalous Hall effect observed for the crystal is an essential nature of EuMnSb₂.

Figures 6(a) and 6(b) show the angular dependence of MR at 2 K when the applied magnetic field is perpendicular and parallel to the a axis, respectively. For the measurements, the gauge current (I) flows along either the b - or c axis. When the in-plane angle ω is intermediate between zero and 90° [Fig. 6(a)], no additional behavior appears except a weak anisotropy. The zigzag chain net of Sb accompanied by the orthorhombic distortion is possibly responsible for the weak in-plane anisotropy of MR.

When the out-of-plane angle θ between H and the a axis varies [Fig. 6(b)], a bump appears at small angles ($\theta = 5^\circ$ and 10°) and disappears at larger θ . This reminds us of the spin-flop transition observed at 2 K [inset of Fig. 2(b)]. An increasing magnetic field seems to switch the weakly anisotropic AFM state to a less anisotropic AFM state via the spin-flop transition. The spin reorientation seems to have an impact on the MR, especially at small angles. To further investigate the relevance among H and M and ρ_{xx} , the data are plotted in other forms [Figs. 6(c) and 6(d)]. The analysis clearly shows a strong connection between the reorientation of the out-of-plane magnetic moments and ρ_{xx} , supporting the fact that spin-flop transition drives the MR anomaly.

IV. CONCLUSIONS

We successfully grew high-quality single crystals of EuMnSb_2 by a Sn flux method. Crystal structure and magnetic and electrical properties were characterized. Unlike other AMnPn_2 compounds, EuMnSb_2 is semiconductinglike, with a very small activation energy of 30.1(4) meV. A broad peak in the ρ - T plot shifts to higher temperature with increasing magnitude of the applied magnetic field, suggesting that the magnetic order is tightly correlated with the charge transport. In addition, a large negative MR was observed at low temperatures, reaching -95% at 2 K.

Although the magnetic properties of EuMnSb_2 were found to be much like those of EuMnBi_2 , the transport properties are

qualitatively different from those of EuMnBi_2 . The observed transport properties of EuMnSb_2 are indicative of a distance between the bulk electronic state and an expected state for a Dirac material. Perhaps the characteristic Sb zigzag chain net, together with the orthorhombic lattice distortion, puts the electronic state of EuMnSb_2 away from the Dirac state [12,13]. However, a recent study of SrMnSb_2 , which has a similar Sb zigzag chain net, shows notable Dirac semimetal behaviors with a positive MR ($\sim 135\%$ at 30 K and 160 kOe) [32]. Therefore, the origin of the qualitatively different transport properties of EuMnSb_2 remains completely unclear and open for future research.

ACKNOWLEDGMENTS

We thank Hongming Weng and Qiunan Xu for valuable discussions. This work was supported by the National Key Research and Development Program of China (Grants No. 2017YFA0302901 and No. 2016YFA0300604), the National Natural Science Foundation of China (Grants No. 11474330, No. 11774399, No. 11574377, No. 11674375, No. 11634015, and No. 61425015), and the Strategic Priority Research Program (B) of the Chinese Academy of Sciences (Grant No. XDB07020000). Work in Japan was supported by JSPS KAKENHI (Grants No. JP15K14133 and No. JP16H04501) and JSPS Bilateral Open Partnership Joint Research Projects. C.Y. and S.Y. contributed equally to this work.

-
- [1] X.-L. Qi and S.-C. Zhang, *Rev. Mod. Phys.* **83**, 1057 (2011).
 [2] M. Z. Hasan and C. L. Kane, *Rev. Mod. Phys.* **82**, 3045 (2010).
 [3] N. Nagaosa, J. Sinova, S. Onoda, A. H. MacDonald, and N. P. Ong, *Rev. Mod. Phys.* **82**, 1539 (2010).
 [4] M. König, S. Wiedmann, C. Brüne, A. Roth, H. Buhmann, L. W. Molenkamp, X.-L. Qi, and S.-C. Zhang, *Science* **318**, 766 (2007).
 [5] B. A. Bernevig, T. L. Hughes, and S.-C. Zhang, *Science* **314**, 1757 (2006).
 [6] J. Xiong, S. K. Kushwaha, T. Liang, J. W. Krizan, M. Hirschberger, W. Wang, R. J. Cava, and N. P. Ong, *Science* **350**, 413 (2015).
 [7] T. Liang, Q. Gibson, M. N. Ali, M. Liu, R. J. Cava, and N. P. Ong, *Nat. Mater.* **14**, 280 (2015).
 [8] Z. Wang, H. Weng, Q. Wu, X. Dai, and Z. Fang, *Phys. Rev. B* **88**, 125427 (2013).
 [9] Z. Wang, Y. Sun, X.-Q. Chen, C. Franchini, G. Xu, H. Weng, X. Dai, and Z. Fang, *Phys. Rev. B* **85**, 195320 (2012).
 [10] X. Huang, L. Zhao, Y. Long, P. Wang, D. Chen, Z. Yang, H. Liang, M. Xue, H. Weng, Z. Fang, X. Dai, and G. Chen, *Phys. Rev. X* **5**, 031023 (2015).
 [11] B. Q. Lv, H. M. Weng, B. B. Fu, X. P. Wang, H. Miao, J. Ma, P. Richard, X. C. Huang, L. X. Zhao, G. F. Chen, Z. Fang, X. Dai, T. Qian, and H. Ding, *Phys. Rev. X* **5**, 031013 (2015).
 [12] M. A. Farhan, L. Geunsiik, and S. Ji Hoon, *J. Phys.: Condens. Matter* **26**, 042201 (2014).
 [13] G. Lee, M. A. Farhan, J. S. Kim, and J. H. Shim, *Phys. Rev. B* **87**, 245104 (2013).
 [14] A. Zhang, C. Liu, C. Yi, G. Zhao, T.-I. Xia, J. Ji, Y. Shi, R. Yu, X. Wang, C. Chen, and Q. Zhang, *Nat. Commun.* **7**, 13833 (2016).
 [15] Y. Feng, Z. Wang, C. Chen, Y. Shi, Z. Xie, H. Yi, A. Liang, S. He, J. He, Y. Peng, X. Liu, Y. Liu, L. Zhao, G. Liu, X. Dong, J. Zhang, C. Chen, Z. Xu, X. Dai, Z. Fang, and X. J. Zhou, *Sci. Rep.* **4**, 5385 (2014).
 [16] Y. F. Guo, A. J. Princep, X. Zhang, P. Manuel, D. Khalyavin, I. I. Mazin, Y. G. Shi, and A. T. Boothroyd, *Phys. Rev. B* **90**, 075120 (2014).
 [17] K. Wang, L. Wang, and C. Petrovic, *Appl. Phys. Lett.* **100**, 112111 (2012).
 [18] J. B. He, D. M. Wang, and G. F. Chen, *Appl. Phys. Lett.* **100**, 112405 (2012).
 [19] K. Wang, D. Graf, L. Wang, H. Lei, S. W. Tozer, and C. Petrovic, *Phys. Rev. B* **85**, 041101 (2012).
 [20] J. Park, G. Lee, F. Wolff-Fabris, Y. Y. Koh, M. J. Eom, Y. K. Kim, M. A. Farhan, Y. J. Jo, C. Kim, J. H. Shim, and J. S. Kim, *Phys. Rev. Lett.* **107**, 126402 (2011).
 [21] J. K. Wang, L. L. Zhao, Q. Yin, G. Kotliar, M. S. Kim, M. C. Aronson, and E. Morosan, *Phys. Rev. B* **84**, 064428 (2011).
 [22] L. Li, K. Wang, D. Graf, L. Wang, A. Wang, and C. Petrovic, *Phys. Rev. B* **93**, 115141 (2016).
 [23] J. Liu, J. Hu, H. Cao, Y. Zhu, A. Chuang, D. Graf, D. J. Adams, S. M. A. Radmanesh, L. Spinu, I. Chiorescu, and Z. Mao, *Sci. Rep.* **6**, 30525 (2016).

- [24] S. Huang, J. Kim, W. A. Shelton, E. W. Plummer, and R. Jin, *Proc. Natl. Acad. Sci. USA* **114**, 6256 (2017).
- [25] H. Masuda, H. Sakai, M. Tokunaga, Y. Yamasaki, A. Miyake, J. Shioyai, S. Nakamura, S. Awaji, A. Tsukazaki, H. Nakao, Y. Murakami, T. H. Arima, Y. Tokura, and S. Ishiwata, *Sci. Adv.* **2**, e1501117 (2016).
- [26] A. F. May, M. A. McGuire, and B. C. Sales, *Phys. Rev. B* **90**, 075109 (2014).
- [27] A. Wang, I. Zaliznyak, W. Ren, L. Wu, D. Graf, V. O. Garlea, J. B. Warren, E. Bozin, Y. Zhu, and C. Petrovic, *Phys. Rev. B* **94**, 165161 (2016).
- [28] K. Wang and C. Petrovic, *Phys. Rev. B* **86**, 155213 (2012).
- [29] K. D. Myers, S. L. Bud'ko, V. P. Antropov, B. N. Harmon, P. C. Canfield, and A. H. Lacerda, *Phys. Rev. B* **60**, 13371 (1999).
- [30] K. Wang, D. Graf, and C. Petrovic, *Phys. Rev. B* **87**, 235101 (2013).
- [31] E. Brechtel, G. Cordier, and H. Schäfer, *J. Less-Common Met.* **79**, 131 (1981).
- [32] J. Y. Liu, J. Hu, Q. Zhang, D. Graf, H. B. Cao, S. M. A. Radmanesh, D. J. Adams, Y. L. Zhu, G. F. Cheng, X. Liu, W. A. Phelan, J. Wei, M. Jaime, F. Balakirev, D. A. Tennant, J. F. DiTusa, I. Chiorescu, L. Spinu, and Z. Q. Mao, *Nat. Mater.* **16**, 905 (2017).
- [33] H. J. Park, L. J. Sandilands, J. S. You, H. S. Ji, C. H. Sohn, J. W. Han, S. J. Moon, K. W. Kim, J. H. Shim, J. S. Kim, and T. W. Noh, *Phys. Rev. B* **93**, 205122 (2016).
- [34] G. M. Sheldrick and T. R. Schneider, *Methods Enzymol.* **277**, 319 (1997).
- [35] See Supplemental Material at <http://link.aps.org/supplemental/10.1103/PhysRevB.96.205103> for additional structural properties, chemical composition and physical properties.
- [36] J. W. Simonson, G. J. Smith, K. Post, M. Pezzoli, J. J. Kistner-Morris, D. E. McNally, J. E. Hassinger, C. S. Nelson, G. Kotliar, D. N. Basov, and M. C. Aronson, *Phys. Rev. B* **86**, 184430 (2012).
- [37] S. Borisenko, Q. Gibson, A. Yaresko, T. Kim, M. N. Ali, B. Buechner, M. Hoesch, and R. J. Cava, [arXiv:1507.04847v2](https://arxiv.org/abs/1507.04847v2).
- [38] S. Nandi, Y. Xiao, N. Qureshi, U. B. Paramanik, W. T. Jin, Y. Su, B. Ouladdiaf, Z. Hossain, and T. Brückel, *Phys. Rev. B* **94**, 094411 (2016).
- [39] V. K. Anand and D. C. Johnston, *Phys. Rev. B* **94**, 014431 (2016).
- [40] I. Schellenberg, M. Eul, W. Hermes, and R. Pöttgen, *Z. Anorg. Allg. Chem.* **636**, 85 (2010).
- [41] O. Prakash, A. Thamizhavel, and S. Ramakrishnan, *Phys. Rev. B* **93**, 064427 (2016).
- [42] Y. Shapira, S. Foner, N. F. Oliveira, and T. B. Reed, *Phys. Rev. B* **10**, 4765 (1974).
- [43] N. Haham, Y. Shperber, M. Schultz, N. Naftalis, E. Shimshoni, J. W. Reiner, and L. Klein, *Phys. Rev. B* **84**, 174439 (2011).